Characterization of chemical composition and particle size distribution of aerosols released during laser cutting of fuel debris simulants

Claire Dazon, Emmanuel Porcheron, Christophe Journeau, Christophe Suteau, Christophe Chagnot, Ioana Doyen, Emmanuel Excoffier, Damien Roulet

Characterization of chemical composition and particle size distribution of aerosols released during laser cutting of fuel debris simulants

C.Dazon[1*], E.Porcheron[1], C. Journeau[2], C. Suteau[2], C. Chagnot[3], I. Doyen[3], E. Excoffier[4], D. Roulet[5]

[1] Institut de Radioprotection et de Sûreté Nucléaire (IRSN), PSN-RES, SCA, 91192 Gif-sur-Yvette, France.

[2] Commissariat à l'Energie Atomique (CEA), DEN, Cadarache, DTN, SMTA, LEAG, F-13108 Saint-Paul-lez-Durance, France.

[3] Commissariat à l'Energie Atomique (CEA), DEN/SEMT, Université Paris-Saclay, F-91191 Gif-sur-Yvette, France.

[4] Commissariat à l'Energie Atomique, DEN/DMRC/SA2I/LMAC, 30207, Bagnols-sur-Cèze, France.

[5]ONET Technologies, 26701 Pierrelatte, France.

*claire.dazon@irsn.fr

Keywords: radioactive aerosol size distribution, Fukushima Daiichi dismantling, laser cutting, corium retrieval

Highlights

- Original data on the characterization of surrogate radioactive airborne particles.
- Smaller particles have non negligible radioactivity.
- Improvement perspectives for dismantling applications stem from the results.

Abstract

We present here the results regarding the characterization of chemical composition and size distribution of aerosols released during laser cutting of two representative fuel debris simulants (Ex-Vessel and In-Vessel scenarios) in air and underwater conditions in the context of Fukushima Daiichi dismantling. The aerosols have an aerodynamic mass median diameter below 1 µm, with particle sizes generally comprised between 60 nm and 160 nm for air cutting conditions, and larger diameters (300-400 nm) for underwater experiments. Regarding the chemical composition, iron, chromium and nickel are mainly found by more than 50% in the samples. When compositions are transposed to radioactivity, taking into account radioisotope inventories 10 years after the accident, it is well evidenced that the radioactivity is carried out by small particles in air condition tests (median size around 100 nm): 50% of the radioactivity is present in particles below 90 nm. Caesium carries the largest part of the radioactivity at all sizes below 1 µm in the case of an Ex-Vessel fuel debris simulant. For the In-Vessel, the aerosol median size for the radioactivity is situated around 100 nm, with 59% of the radioactivity is carried by strontium, 17% by barium and 16% by minor actinides (modelled by cerium) and 7% by the caesium. For sizes above 1.6 µm, cerium representing alpha particles (surrogate of plutonium) is almost the only radioactivity-bearing element (96-97% of the radioactivity). The data produced here could already be used in the development strategies to implement in-situ the laser cutting for fuel debris retrieval.

Introduction

One of the important challenges for the dismantling of the damaged reactors of the Fukushima Daiichi Nuclear Power Plant is the retrieval of the fuel debris, also called solidified corium. Corium is the general term used to qualify the molten material composed of complex chemical compounds gathering both radioactive fuel materials and the materials of the reactor structures [1]. Depending on the scenario of the severe accident that occurs in each reactor, the fuel debris are located outside (Ex-Vessel corium) or inside (In-Vessel corium) the reactor pressure vessel. In the particular Ex-vessel case, the molten corium is likely to have interacted with concrete. Fuel debris may have a large range of composition, both at microscopic and macroscopic scale [2] depending on the history of each debris during the accident scenario [3, 4].

Among several techniques for fuel debris retrieval, cutting methods in air and underwater conditions are primordial to investigate such as grinder, laser, plasma torch, arc air, arc saw, reciprocating saw. In particular, the experience from stainless steel cutting indicates that the laser technique is well adapted to the cutting of expected material such as fuel debris compared to the other ones previously mentioned [5]. Preliminary experiments carried out with fuel debris simulant materials by the authors confirmed this good cutting ability for fuel debris [6]. Among the laser benefits, laser cutting technology can be implemented in air and underwater conditions, also in very strong radiating and contaminated environment, it limits the mass fraction of particles released compared to other thermal techniques, it can be controlled remotely and is contactless, removing the risk of blocking a tool in fuel debris.

In addition to study the technological aspects regarding the capability of the cutting tool to be deployed in radiating environment, the risk of the fuel debris retrieval operations has to be assessed to limit dissemination outside the containment vessel, especially in the unlikely case of containment breach during retrieval operations. Therefore, the aforementioned strategies for fuel debris retrieval by cutting methods should put a stress on a high level of security both to

reduce as most as possible the risks of contamination by radionuclides and dissemination into the environment, and protect workers in charge of dismantling.

One of the key point to obtain a relevant assessment of the aerosol dispersion that can lead to radionuclides release during cutting of fuel debris, is to well characterize the aerosol source term. This characterization is crucial since data can be used to predict their transport and deposition by the mean of numerical simulations. In addition, those data are necessary to develop and optimize technologies to ensure the containment, the collection and the filtration of particulate pollutants to avoid human and environmental contamination.

In this view, the important aerosol characteristics to know are the morphology of the particles, their size distribution, the aerosol mass concentration and their chemical composition related with the radioactivity it would carry out for actual fuel debris. Only a specific fraction of particulate matter (PM) penetrates in the human body by the respiratory tracts. In particular, the particle size having 50% of penetration for the respirable fraction is 4 μm aerodynamic diameter, corresponding to the penetration in the deepest region of the human lung [7] and it is an aerosol particle size typically expected for cutting techniques [8]. Concerning the chemical composition associated to the respirable fraction of aerosols (or other conventional fractions as the inhalable or thoracic fractions [7]) in such dismantling context, very rare works dealt with the characterization of both chemical composition and particle size distribution when radiating material (or simulant) is cut. However, it is critical to understand the radionuclides distribution during nuclear power plant decommissioning to prepare and implement fuel debris retrieval by cutting tools such as laser or other means in safety conditions. One can highlight the recent works by Dodds and Rawcliff [9] in which data on the radionuclides distribution during laser cutting of stainless steel in a simulated nuclear decommissioning scenario were produced. The results obtained in their work do not give a lot of information regarding the radionuclides distribution of aerosols released, and many radionuclide concentrations were under the detection limit (ICP-MS analysis). Another study by Chae *et al* [10] analyzed the literature related to characterization of aerosols in terms of size distribution and chemical composition

during cutting of stainless steel materials with mechanical tools, laser or plasma. The radionuclides concerned by this study were the main radioisotopes which can be associated to the reactor materials when the nuclear reactor will be shut down (table 1 [9]). The author evidenced that the aerosols have a notable polydispersity any cutting methods given, with a clear release of ^{60}Co, and fine particles largely under 1 µm in terms of mass size distribution. They evidenced also that the cutting method and the cutting conditions (in air or underwater) affect the chemical composition and the radioactive contamination.

The authors suggested that the underwater cutting condition could minimize the aerosol released in the workplaces and decrease so the internal dose of aerosols potentially inhaled. Besides, the authors highlight the deficiency of radioactivity distribution data for internal dose calculations, even if non-radioactive simulant could be relevantly used for supplanting this lack of information. This metrology issue is largely commented throughout the article, and it appears that a good knowledge of the performance of high-resolution detector for size distribution is required. The reproducibility verification of aerosol distribution data is also stressed on by the authors, evidencing the lack of such essential strategy to obtain relevant aerosol characterization. However, these two works focused on specific material (stainless steel) which does not represent fuel debris. Knowing the influence of cutting methods and initial chemical composition based on the Chae *et al* analysis [10], we can reasonably assume that the literature results concerning the stainless steel cannot be directly transposed to the nuclear fuel debris case.

In this context, this paper aims at (i) presenting original data related to characterization of chemical composition and particle size distribution of aerosols released during laser cutting of fuel debris simulants, (ii) pointing out the relevancy of such approach combining chemical and size distribution aerosol characterization, and finally (iii) proposing perspectives to improve aerosol characterization for future experiments and potential in-situ applicability in the on-going projects. These data were produced throughout research and development projects

subsidized by the Japanese government and carried out by a French consortium (ONET Technologies, CEA, and IRSN) to study and prepare operations of the fuel debris retrieval.

After presenting the fuel debris simulants, the laser cutting technology developed on the DELIA facility and the strategy used for aerosol characterization, we will comment the results related to the chemical elements released during laser cutting and comparison with thermodynamic calculations. Then, we will focus on the particle size distribution of the chemical elements and the transposition to radioactivity with a special attention for uranium based on a computer simulation.

Material and Methods

2.1 Fuel debris simulants

In the project, two types of fuel debris simulants for laser cutting were designed to represent Ex-Vessel and In-Vessel scenari of fuel debris progression. The Ex-Vessel fuel debris simulant composition was determined by CEA [2, 11] from calculations by Japanese and International experts on an Ex-Vessel scenario with molten core concrete interaction in the sump of Fukushima Daiichi unit 1 (1F1) pedestal (configuration maximizing the fraction of concrete decomposition products) including the fission products inventory 10 years after the accident. The In-Vessel fuel debris simulant composition was determined from the average of the Fukushima Daiichi unit 2 (1F2) lower head debris composition calculated within the OECD/BSAF project in which the fission products inventory 10 years after the accident [12] was considered. As described by Journeau and co-workers [2], uranium was simulated by hafnium, plutonium and minor actinides by cerium, whereas the fission products were considered in their natural isotopic composition of the respective chemical elements. Hafnium has been considered as surrogate for uranium as the thermal properties of hafnium oxide (HfO_2 or hafnia) and uranium oxide (UO_2) are quite close [13]: melting points at respectively 3063 and 3033 K; thermal conductivities in solid state close to 2 $W.m^{-1}.K^{-1}$ and heat of fusion of the order of 100 ± 30 $kJ.kg^{-1}$ for both oxides; and specific densities at room temperature of 9 680 and 10 500 $kg.m^{-3}$. Concerning the plutonium, Capriotti *et al.* [14] have shown that "many similarities exist between the system Pu-O and the system Ce-O, even in the very high temperature behavior" and that "CeO_2 displays […] melting behavior which has been recently proven to be typical of other similar metal-oxygen systems such as Ca-O, Np-O and Pu-O". Therefore cerium can be selected as a surrogate for plutonium and minor actinides.

In the case of Fukushima Daiichi reactors, fuel debris can be represented by the general chemical formulation UO_2-$ZrO_{2\pm x}$-X. UO_2-$ZrO_{2\pm x}$ is enriched with a complex part X, gathering all metals and metals oxides that can be encountered by the corium (macroscopic state of fuel debris when accident

occurred) when progressing outside or inside the vessel pressure. In the case of Ex-Vessel scenario, the X composition of corium is more oxidized, in particular by the concrete compounds such as SiO_2, Al_2O_3, CaO or water contained inside, encountered during the Ex-Vessel progression outside the reactor. For the In-Vessel scenario, the corium is less oxidized and it is composed of a X with more metal phase (typically stainless steel) and suboxidized zirconium oxide.

Figure 1 represents the two theoretical fuel debris compositions established for the project by CEA Cadarache for the two scenari. For readability, we do not display all the chemical compounds used in the formulation.

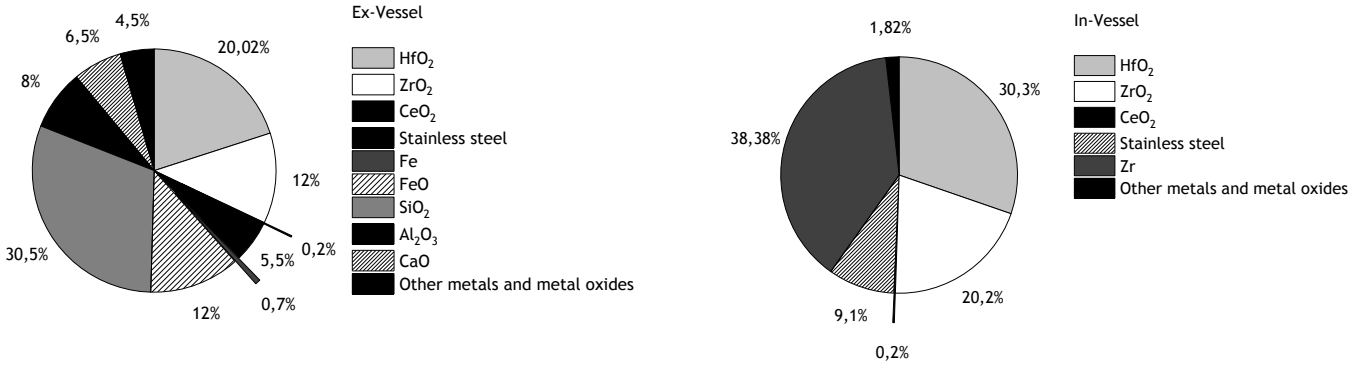

Figure 1 : Theoretical chemical compositions of fuel debris simulants determined by CEA Cadarache.

The other metals and metal oxides in the case of Ex-Vessel simulant (wt%) are the following: B_4C (0.20%), Nd_2O_3 (0.090%), Cs_2O (0.050%), Ba (0.035%), La_2O_3 (0.025%), MoO_2 (0.085%), PdO (0.025%), Pr_2O_3 (0.025%), Sm_2O_3 (0.015%), Y_2O_3 (0.010%), TeO_2 (0.010%), Fe_2O_3 (3.0%), Cr_2O_3 (0.60%) and Sr (0.015%).

In the case of In-Vessel simulant, the other metals and metal oxides are (wt%): B_4C (1.0%), Nd_2O_3 (0.10%), Cs_2O (0.070%), Ba (0.040%), La_2O_3 (0.035%), MoO_2 (0.45%), SnO_2 (1.0%), PdO (0.030%), Pr_2O_3 (0.030%), Sm_2O_3 (0.020%), Y_2O_3 (0.015%), TeO_2 (0.015%) and Sr (0.020%). As previously mentioned, uranium was replaced mole by mole by hafnium and plutonium by cerium.

The fuel debris simulants were synthesized on the PLINIUS platform at CEA Cadarache according to a melting process based on induction heating described in several papers [15, 16, 17]. Briefly, it

consists in inserting the different chemical compounds in powder form (except stainless steel and metallic zirconium) inside a cylindrical magnesium-stabilized-zirconia crucible (180 mm internal diameter and 290 mm high). The crucible is surrounded by a copper induction coil. Protective zirconia powder has been installed around the crucible to provide thermal insulation and to collect melt in case of leakage. Nitrogen gas flow has been provided at the upper surface to simulate the nitrogen atmosphere of the primary containment vessel and prevent significant melt oxidation by air. A hood has been installed above the crucible to collect fumes and aerosols. It is connected through a filter and a HEPA filter to the building chimney. Heating electrical currents have been induced first to the steel balls acting as a susceptor since the metal oxides are not electrically conductive materials at low temperature. The load temperature progressively increased, leading to progressive melting of the powders. When high temperatures have been reached, partial evaporation of volatile compounds occured as during a severe accident. When heating has been finished, the fuel debris were cooled and put off the crucible. Around 10 kg for the Ex-Vessel and 12.5 kg for the In-Vessel simulant of load were used for the synthesis. More details concerning the material elaboration with PLINIUS platform are available in literature [2,11]. After synthesis, the materials were characterized in terms of chemical compositions by ICP-MS and it was shown that the chemical compositions of both simulants were enough close to the expected ones presented above in figure 1. Considering the inner core composition (which is the average of 7 subsample analyses) and the aerosol collection during the melting phase, release fractions during fabrication have been assumed in order to fit the observations and analyses for each element [11]. Less than 2% of the Ex-vessel initial load mass has been volatilized for most elements except for molybdenum (10%), lanthanum (20%), tin (30%), praseodynum (35%) cesium (40%) and tellurium (90%), These releases are compatible with the knowledge on fission product releases [18].

In the Ex-vessel sample, as the corium-concrete mixture density is significantly lower than that of steel, a steel ingot has been found at the bottom of the crucible and has been removed before cutting operations. On the opposite, the density of metallic and ceramic liquid phases in the In-vessel corium are quite close, so that both phases must have been mixed. Indeed, in the solidified fuel debris

simulant, solidified drops of metal have been found as inclusion in the ceramic phase. From chemical analyses, it can be considered that 91 wt% of the original load formed the ceramic phase, 5 wt% the metallic inclusions (mainly Zr, Fe, Hf, Cr) and 4% have been volatilized during fabrication. This leads to local heterogeneities in the fuel debris simulant.

Figure 2 are photographs of the fuel debris simulants obtained on the PLINIUS platform. The simulants were then used on the DELIA facility for laser cutting and aerosol characterization.

Figure 2 : (left) Photograph of Ex-vessel black in its crucible. Cut views of Ex-Vessel (center) and In-Vessel (right) fuel debris simulant synthetized at the PLINIUS platform.

2.2 DELIA facility: laser cutting and aerosol characterization

The concept of the DELIA facility (French acronym for: in air and underwater laser cutting cell) for laser cutting and aerosol characterization is illustrated on figure 3 [19]. DELIA is composed of two sections, one dedicated to laser cutting « aerosol generation », and the second to "aerosol characterization". These sections are separated on three floor levels, the aerosol generation being located at the first and second stages.

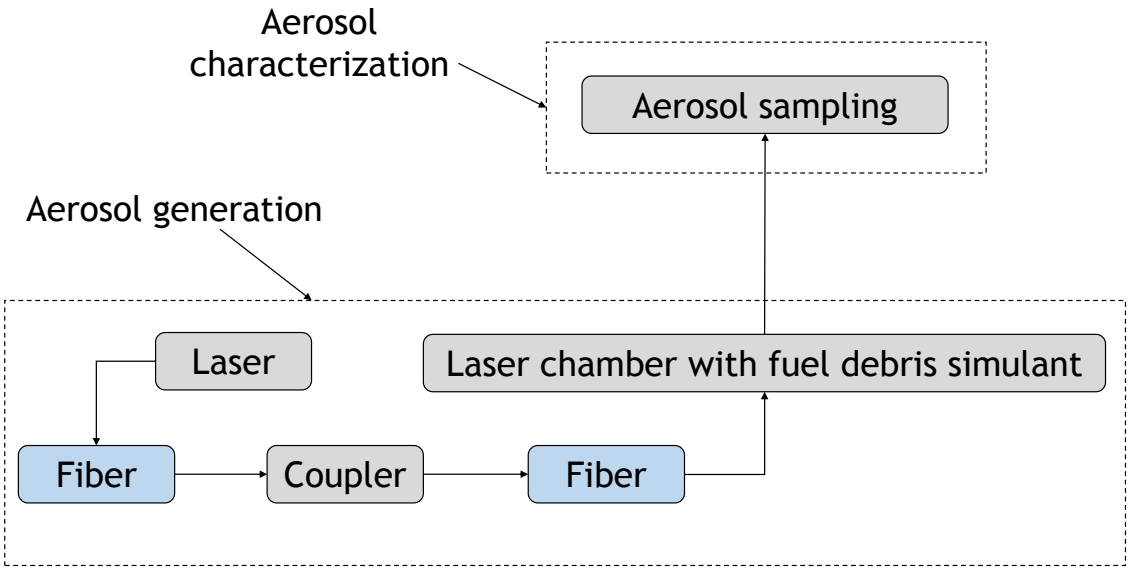

Figure 3 : General diagram of the DELIA facility for laser cutting and characterization of aerosols released.

The next paragraphs will briefly describe the different sections of the DELIA facility and present arguments for aerosol metrology. The last paragraph will sum up the test grid implemented and the post-test analysis.

2.2.1 Description of the DELIA facility (aerosol generation)

The « aerosols generation » section of DELIA is illustrated on figures 4 and 5, and was described in literature by Chagnot *et al* [19]. Briefly, the continuous laser (TRUMPF company) delivers a beam with a power of 8 kW at a wavelength of 1.03 µm to the laser head. Several laser heads have been considered. In this work, the laser head used for in air cutting was cooled by pressurized air, whereas a laser head cooled water was used for underwater cutting. Laser cutting is obtained by both the action of the focused laser beam on the material work piece and the mechanical action of the assisting gas jet acting co-axially with the laser beam. The air passing through the laser lets aerosol transport in the upper chimney connected to the aerosol sampling line. The cutting speed is set as a function of the thickness of the piece and its physico-chemical properties (in particular, melting point).Two chimneys are positioned on the upper part of the cutting cell, one of them with a 300 mm diameter is used for the exhaust of the aerosol and the gas. Finally, the cutting cell can be filled with water until 5 m height.

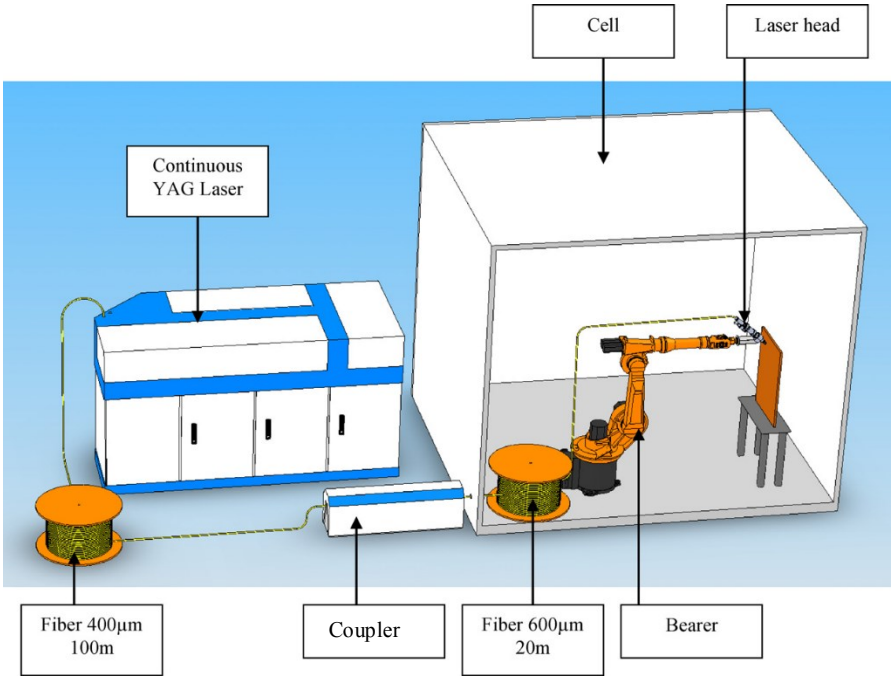

Figure 4 : Sketch of the laser cutting installation in the DELIA facility in a case of in air cutting site (aerosol generation part- (Figure 1 Chagnot *et al* [19]). The cutting cell is a stainless tank (1.38 m in diameter and 3 m length, 3.7 m^3 usable volume, 5 m^3 with chimneys).

Figure 5 **:** View of the cutting cell of the DELIA facility.

2.2.2 Description of the aerosol sampling line (aerosol characterization) and arguments for aerosol metrology

The aerosol source term characterization is performed using a specific test section implemented on the top floor of the DELIA facility. This characterization is carried out through the measurements of the mass concentration, the particle size distribution and the composition of the aerosols that are sampled in the aerosol test section connected to the exhaust line of the DELIA laser cutting cell (Figure 6) [20]. Different instruments are implemented on the aerosol test section to provide together real time and integrated measurements of aerosol characteristics (Figure 7). The positions of these instruments in the test section are depicted in the Figure 7. All mechanisms involved in the transport and particle deposition in the cylindrical sampling line have been integrated in a numerical tool (AEROCALC [21]). This software can calculate, for different kinds of geometries and singularities, the aerosol deposition fraction in the sampling line (or aerosol penetrating fraction) according to the flow conditions and aerodynamic diameters of particles. For the smallest aerodynamic diameters, 0.03 µm and 1 µm, the penetrating fractions are equal to 99 %, meaning that the losses in the sampling line up to the different instruments are negligible.

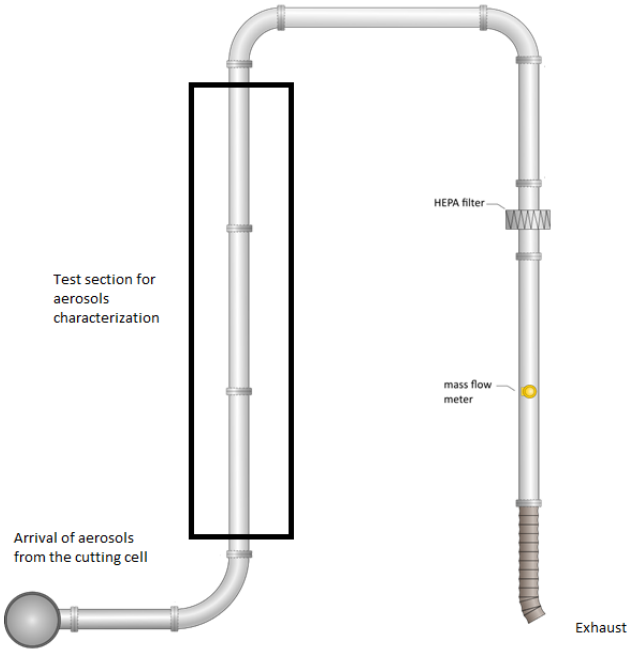

Figure 6 : Sketch of the loop dedicated to aerosols sampling.

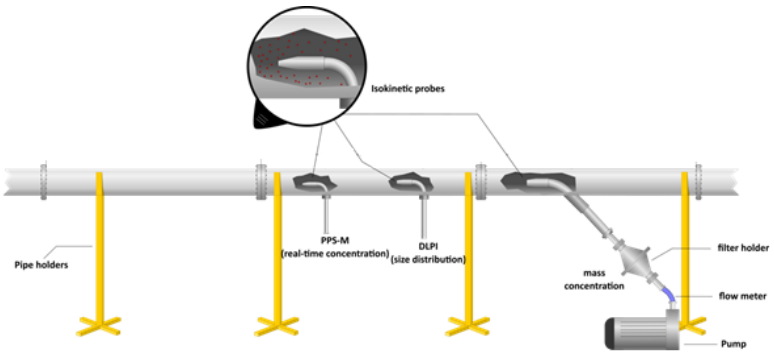

Figure 7 : Test section for aerosols measurements.

The physical quantities regarding airborne particles measured during laser cutting tests are the following [20]:

- the mass concentration of the aerosol by filter sampling,

- the time evolution of the aerosol mass concentration using a Pegasor PPS-M® aerosol sensor,
- the particles size distribution according to the aerodynamic diameter using a Low Pressure Impactor (DLPI®, Dekati),
- the volume flow rate in the exhaust line,
- the pressure drop of the HEPA filter positioned downstream in the exhaust line,
- the qualitative chemical composition of the collected particles on sampling filter using a coupled analysis of Scanning Electron Microscopy *(*SEM) or Transmission Electron Microscopy (TEM) and Energy-Dispersive X-ray Spectroscopy (EDS) analysis.

Aerosol concentration is an important data to measure. Beyond the simple information on the quantity of particles released, the application can be multiple as aerosol concentration generally manages the aerosol measurement procedure in several research and industrial areas. The aerosol concentration can be done throughout filter sampling techniques or real time measurement devices relying in general on optical principle [21]. The usually-used metrics are the number and mass concentrations.

Filter sampling techniques are the most simple and commonly used techniques to determine the mass concentration of particle in a flow. Membrane filtrations have been developing for more than 20 years now, in order to offer, as most as possible, reliable media for robust results for aerosol collection taking into account the environmental conditions of sampling [22, 23, 24, 25]. In the DELIA facility, it appeared that the simplest way to assess the global aerosol concentration during a laser cut was the filter sampling, leading so to mass concentration measurement. A robust air sampling filtration in the DELIA facility required the following elements concerning the medium used in this view:

- strength to the high flowrate between 100 and 400 L/min (in air cutting) or 2000 L/min (underwater cutting),

- insensitivity to the humidity in the sampling line which can be comprised between 90% and 100% during tests conducted underwater,
- low limit of detection,
- collection efficiency higher than 98%.

Some recent studies [22, 23, 24] demonstrated the high robustness of quartz fiber collection media regarding the conditions mentioned above, and more generally, inorganic matrices are well adapted to any type of aerosols. These media can also be used for post-test analysis (SEM or TEM, chemistry).

By consequence, we chose to implement quartz fiber collection media to measure the global aerosol mass concentration on the DELIA facility.

Cascade impactors are instruments of choice for the determination of aerosol mass size distribution in the expanded range 0.03 µm –10 µm, which is a sufficiently wide range to assess all the particle sizes expected during laser cutting. The particle size distribution is directly expressed in mass as each quantity of particles impacting the plates of the instrument is weighted. Particles are selected by the different plates of the impactor depending on their aerodynamic diameter, equivalent diameter which is directly used in transport and particle deposit calculations. Remaining particles that were not collected on the cascade impactor plates are collected by filtration in the instrument [21]. Moreover, the cascade impactor can work with high concentrated aerosols. It is important to characterize the size distribution according to the aerodynamic equivalent diameter of the particles released during laser cutting in order to have a better management of the potential occupational and environmental exposures. Indeed, main deposition mechanisms are based on this type of diameter metrics. The DLPI® device is adapted for such size distributions assessment since it gives access directly to the equivalent aerodynamic diameter.

Finally, the Pegasor Particle Sensor (PPS-M®) is a robust and simple device, usually used to measure aerosol concentrations coming from combustion sources or engine exhaust, but it is not limited to this area. Pegasor PPS-M® is based on the “escaping charge” principle to measure the

number and mass concentrations of nanosized to microsized particles [26, 27]. Thanks to calibration factors for specific type of aerosols, the PPS-M® is able to give both number and mass concentrations. This is of particular interest for the project as real-time number concentration of aerosols released helps to manage the tests conducted, and the mass concentration can strengthen the results obtained with the air sampling with the quartz filter. Moreover, the PPS-M® is a compact instrument, and has a very low response time (< 0.3 s). All of these characteristics lead us to choose Pegasor PPS-M® for real time number and mass concentrations of aerosols emitted on the DELIA facility.

2.2.3 Test sequence, aerosol parameters and post-test analysis

The test sequence in the DELIA facility for laser cutting is the following:

- the simulant of fuel debris (Ex-Vessel or In-Vessel one) is implemented in the cutting cell in front of the laser head,
- the cutting cell is closed and the gas injection through the laser head is started (flow rate equal to 120 $m^3.h^{-1}$ (2000 L/min underwater),
- the aerosol measurements in the test section are started in order to determine the background noise regarding the aerosol concentration before the start of the cutting,
- the laser cutting starts (the laser is started at the reference time t=0 s) with the tuned cutting parameters such as the cutting speed and the laser power (8 kW),
- the acquisition of the aerosol measurements is performed during the cutting,
- the laser cutting is stopped but the gas injection through the laser head continues,
- the acquisition of the aerosol measurements is still performed until reaching a similar level for background noise comparatively to the beginning of the test.

The repeatability of the measurements regarding the aerosol number concentration and the aerosol size has been checked. For those specific tests, zirconia material has been used as fuel debris simulant in order to have a material with homogeneous composition and regular shape (parallelepiped block). The results presented in other communication [20] demonstrated a good

repeatability in the production of aerosols with the laser cutting in terms of size distribution, mass and number concentration.

Table 1 displays the test grid implemented on the DELIA facility with the fuel debris simulant in air and underwater conditions. Table 2 gathers the aerosol properties measured with each instrument presented above and the associated conditions. These information were applied for each test presented in table 1. The quartz filters and DLPI® aluminium foils were analysed after weighing (mass concentration obtained on the filter and each DLPI® stage, Sartorius® MC 210 P microbalance) by CEA Marcoule with Inductive Coupled Plasma (ICP-MS) (AES (iCap 7300) and MS (iCap Q) Thermo Fisher Scientific), according to an intra-laboratory procedure based on acidic digestion of the substrate. 23 chemical elements researched were: Hf, Zr, Ce, Sn, B, Cr, Fe, Ni, Si, Al, Ca, S, Nd, Mo, Cs, Ba, La, Pd, Pr, Sm, Sr, Y, Te. Aluminum (for DLPI® collection substrates) and silicon (for quartz filters) were not considered in the quantification since these elements constitute the substrate matrices. Moreover, let us highlight that neither ICP-MS nor ICP-AES distinguishes whether chemical elements are part of a metallic phase or an oxidized phase as for instance iron (Fe can be present as metallic iron or as oxides FeO, Fe_3O_4, Fe_2O_3). The relative uncertainty associated to ICP-MS measurement was assessed to ± 10% for each element.

The mass concentration, C_M, is determined according to equation 1, where Δm is the net mass measured on the filter or on the substrate and V_M the sampled volume (this term combines the sampling flowrate for each apparatus and the sampled time, typically comprised between 90 and 120 seconds):

$$C_M\,(mg.m^{-3}) = \frac{\Delta m\,(mg)}{V_M(m^3)} \quad (1)$$

Table 1: Test grid implemented on the DELIA facility for laser cutting of fuel debris simulants. The uncertainties correspond to one standard deviation (n = 3 tests).

Simulant	Test N°	Thickness (mm)	Water depth (m)	Cutting Speed (cm/min)
Ex-Vessel	1	20-25 ± 1	-	10 ± 0.5
	2	20 ± 1	0.35 ± 0.1	10 ± 0.5
	3	20 ± 1	5.6 ± 0.1	10 ± 0.5
In-Vessel	4	30 ± 1	-	6 ± 0.5
	5	30 ± 1	0.35 ± 0.1	6 ± 0.5
	6	30 ± 1	5.6 ± 0.1	6 ± 0.5

Table 2: Aerosol metrology parameters used for air and underwater conditions on the DELIA facility. Sampling time for filter and DLPI® was adjusted to few minutes to limit the saturation of collection media with potential high concentrated aerosols.

Aerosol property	Instrument	Conditions
Number (#/cm^3) and mass (mg/m^3) concentration	Sensor Pegasor PPS-M®	Sampling flowrate : 5.6 L/min
Mass size distribution (30 nm – 10 µm)	DLPI® (Dekati)	Sampling flowrate : 30 L/min Use of aluminium foils as collection substrates, previously greased with Apiezon-L to limit particle bounce
Mass concentration (mg/m^3)	Filter sampling (100% Quartz fiber Whatman® QM-H)	Sampling flowrate : 120 L/min
Aerosol chemical composition	ICP-MS and ICP-AES (post-test)	Chemical analysis of the quartz filter and DLPI® collection media after sampling

For this paper, we chose to present the results regarding filter sampling, mass size distributions and chemical characterization of the filter and the collection plates of the DLPI®. PPS-M®, SEM, TEM and EDS will not be discussed here.

Results and discussions

3.1 Comparison between filter sampling and DLPI®

In this work, a first interesting comparison relies on the DLPI® and filter mass concentration and chemical elements detected. Table 3 compares the global mass concentrations obtained on the quartz filter and the DLPI® (summing of the mass concentration of the 13 collection substrates of the impactor) after sampling. We do not present the results related to the 5.6 m underwater conditions due to quantity of deposited matter below the limit of detection of the microbalance.

Table 3: Global mass concentrations obtained for Ex-Vessel and In-Vessel aerosols produced after laser cutting in air (A) and underwater (U) conditions. The uncertainties indicated represent 2 standard deviations for 3 successive filter or collection substrate weighings.

Simulant	N° test	Sampling time (s)	Filter ($mg.m^{-3}$)	DLPI® ($mg.m^{-3}$)
Ex-Vessel	1 (A)	90	31.17 ± 5.94	32 ± 2.78
	2 (U)	120	55.55 ± 3.96	42.68 ± 4.67
In-Vessel	4 (A)	120	226.64 ± 9.89	166.34 ± 13.32
	5 (U)	< 120	145.28 ± 5.74	100.04 ± 7.53

One can observe that in air and underwater conditions, the Ex-Vessel cutting generates less mass concentrations (filter or DLPI®) than the In-Vessel case. In air conditions, the In-Vessel cutting entails between 5 and 7 times more aerosol mass concentration than in the Ex-Vessel case. For underwater conditions, the In-Vessel generates around twice more aerosol concentration. However, one can note that under 0.35 m of water, the aerosol mass concentrations are higher for Ex-Vessel than in air cutting

(filter and DLPI®, around 50% of increase) whereas we can observe a decrease for the In-Vessel (around 60% of decrease).

Even if the laser cutting head creates a large gas bubble between the head and the sample, the presence of water will modify the oxidation state of the melting material. This will affect the vaporization process and thus the generation of aerosols. The main mechanism influencing the aerosol transfer above the water level is the transport by rising bubbles seeded with aerosols during the cutting process. During this phase, interactions with water occur, leading to aerosols collection by water. In addition to aerosol transport by bubbles, other mechanisms leading to aerosol transfer from the water to the gas have to be considered. Due to the high gas flow rate injected through the laser head, the water surface suffers from a strong agitation. The deformation of the liquid – gas interface entails production and ejection of water droplets into the atmosphere. Because the water is continuously seeded with particles during the laser cutting, the droplets ejection may provide aerosols resuspension when droplets become dried. Nevertheless, we point out that the case of 5.6 m of water did not lead to correctly assess the mass concentrations (limit of detection), which can be considered as a proof of significant scrubbing of aerosols by 5.6 m of water.

Concerning the filter and DLPI® comparison, the biases concerning the mass concentrations are relatively low and acceptable taking into account the uncertainties. Indeed, the bias between filter and DLPI® mass concentration (filter taken as reference) for Ex-Vessel laser cutting in air is hardly 2.6%. For the other conditions, the biases are comprised between -30 and -20%, the DLPI® mass concentrations being systematically lower than those of the filter. This can be explained, for a part, by possible particles rebound and/or overload collecting substrate. Indeed, when DLPI® collecting substrates are overload, it is possible that particles collected on a given stage pass in the inferior or superior stage and entail incorrect mass distribution analysis. This phenomenon is limited by the collection substrate greasing (Apiezon-L) but very high aerosol concentration can induce even so the overloading and particle rebound.

Figure 8 displays parity plot graphs comparing the total relative masses for each chemical element detected by ICP-MS and AES on the DLPI® collection substrates and quartz filter. The uncertainties for each element dosed (one standard deviation) correspond to ± 10% of the value.

The best comparison we can observe concerns the laser cutting for Ex-Vessel in air and underwater conditions. Indeed, the ratio of the relative mass for the whole DLPI® channels and the filter mass for each element is generally comprised between 0.7 and 1.5 except the elements detected in very low concentrations. In particular, one can see that for several elements in air conditions: La, Nd, Pr, Sm, Sn, Sr, Te, Y for which the concentrations obtained with ICP-MS are under the limit of detection of the technique (10^{-4} %), the results cannot be robustly compared with the filter. For underwater conditions, these elements are detectable, but remain in very low concentrations (< 0.01%).

The most abundant elements in Ex-Vessel aerosol, both in air and underwater conditions are those coming from stainless steel: iron, chromium, nickel; and those related to concrete such as calcium. We mentioned that silicon and aluminium were not integrated in the quantification since they constitute an important part of the matrices, respectively for the filter and the aluminium foils of the DLPI®. If we could have measured by ICP-MS series of blank substrates, it could have been interesting to substitute the initial aluminium and silicon content of the matrices to the different samples in order to finally quantify the silicon and aluminium elements. These quantifications could have put a stress on the real presence of the concrete elements Al and Si in the aerosol with significant values (> 0.1%). Finally, one can note the presence of barium, caesium, cerium, hafnium, palladium, tin and zirconium in detectable concentrations around 0.1%, these latter being carriers of potential radioisotopes with hafnium representing uranium and cerium plutonium.

For In-Vessel, in both conditions (air and underwater), the results are generally more scattered, and no tendency seems to be drawn. This can be attributed to the larger heterogeneity of the In-Vessel sample, due to the inhomogeneous repartition of the metallic droplets. The DLPI® overestimates or underestimates the relative mass concentrations of the chemical elements, and biases compared to the reference quartz filter can be upper than 100%. The ratio of the relative mass for the whole DLPI®

channels and the filter mass for each element is generally comprised between 0.1 and 800 with iron, chromium, hafnium, cerium, molybdenum, barium, and praseodymium characterized by ratios between 0.7 and 1.3. As for the Ex-Vessel, In-Vessel aerosol is characterized by a predominance of the stainless steel elements, and less presence of radioisotopes, even if hafnium and palladium remain upper than 0.1% concentration based on the filter results.

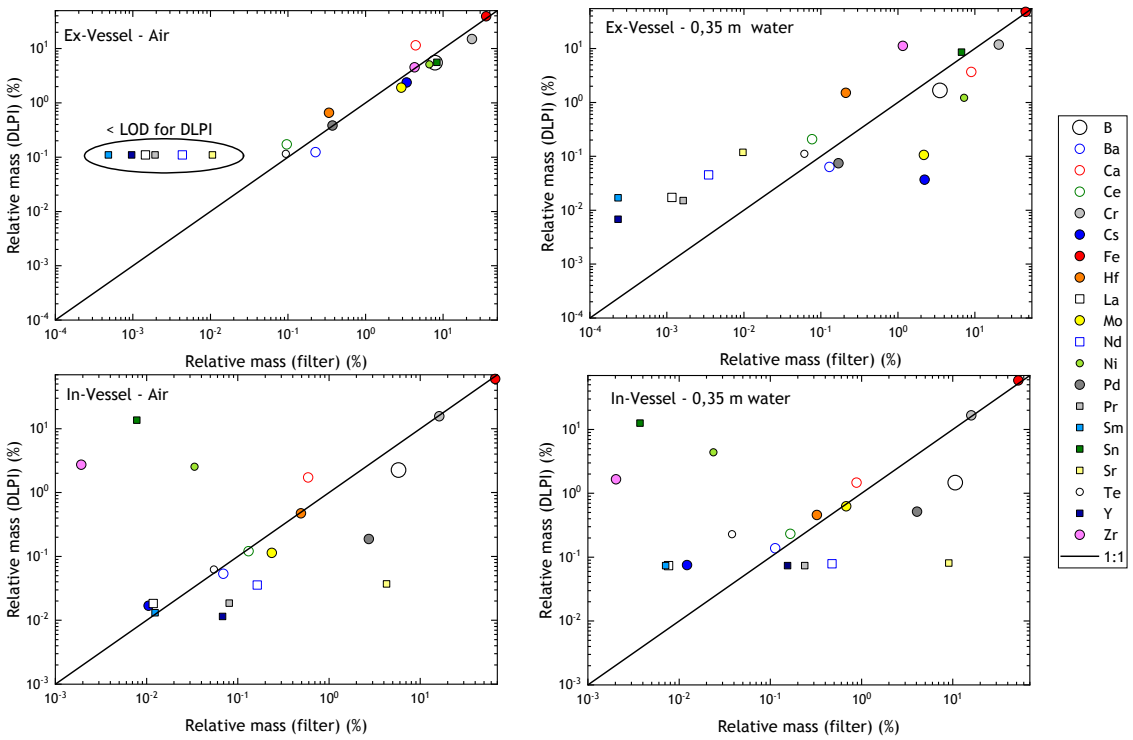

Figure 8 : Parity plots comparing relative mass of each chemical element researched on the filter and DLPI® for Ex-Vessel and In-Vessel laser cutting in air and underwater conditions. The results under the limit of detection are displayed at 0.1% in order to read the filter concentrations, but the results cannot be interpreted. Error bars (not visible) correspond to ± 10% of the values.

The chemical analysis by ICP-MS cannot lead to distinction between oxidic phase and metallic phase. The initial composition of the Ex-Vessel fuel debris simulant includes, for instance, oxidized iron (FeO, Fe_2O_3) and metallic part (stainless steel balls). The iron dosed by ICP-MS includes all the iron states, both the oxidized and metallic elements. Moreover, the laser cutting is likely to entail oxidation and nitration of the metals, which is not clearly evidenced in the results presented here. It could have been interesting to complete this aerosol characterization by X-Ray Diffraction and X-Ray Fluorescence post-analysis on the collection substrates and quartz filter in order to dose the major

oxidized compounds and evidenced their crystalline structure. XPS could also be used for surface analysis of the collection substrate to characterize the chemical environment of the elements and semi-quantify their structure. These analyses could evidence the potential chemical reactions occurring during laser cutting. This point could be considered in the future for next phases of the projects.

3.2 Thermodynamic calculations

It has been assumed that the aerosols are formed from the condensation of the vapors produced by the fuel debris when it is heated by the laser beam as considered in previous works on aerosols over a molten corium pool [30]. Thermodynamic equilibrium calculations have been carried out using GEMINI2 and the NUCLEA14 database. These calculations assume that the molten material is at a homogeneous temperature which is fitted with experimental results. Oxygen and argon are added to represent air neglecting potential effect of nitrides entailed by nitrogen presence. Nitrogen is unavailable in the database, letting us suppose that only oxidation occurs and oxidized compounds are released. Some elements have been substituted by others, mole by mole, because they are not present in the database: zirconium replaces hafnium, chromium replaces molybdenum, lanthanum is surrogate for praseodymium, cerium, yttrium, samarium, neodymium, silver replaces tellurium and palladium, indium is simulating tin. 15 wt% of air have been determined by trial and error to best fit the measured composition for the major elements. For this composition, the liquidus temperature has been computed to be around 1980 K.

Figure 9 shows the measured proportions of the major elements released for an Ex-Vessel modelling. The major element is iron followed by chromium, tin and boron. Assuming equilibrium at 2800-2900 K (800-900 K above the liquidus) provides a reasonable correspondence between calculation and experiment, except for Ni which is overestimated in these calculations. The major computed vapor phases at 2800 K are BO_2 (5 mbar), SiO (3 mbar), Ni (2 mbar), CrO_2 (1 mbar), B_2O_3 (1 mbar) and FeO (1 mbar).

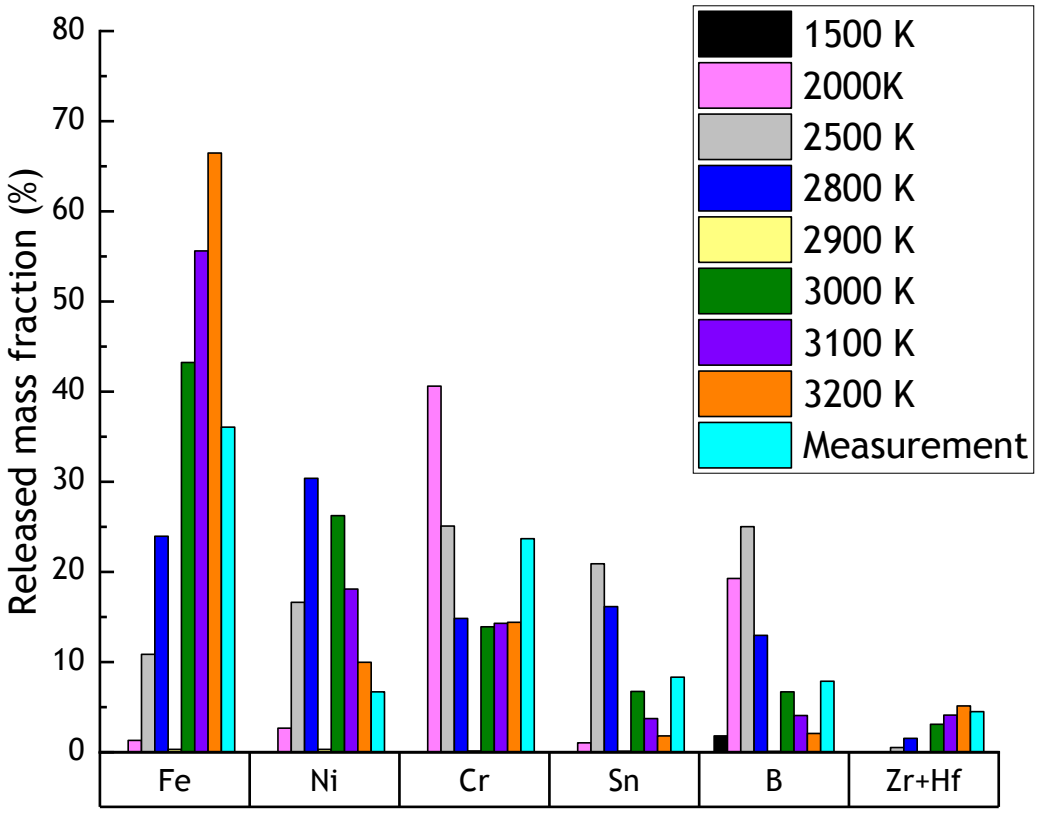

Figure 9 : Calculated mass fractions (major elements) of aerosol released for an Ex-Vessel case study and for different temperatures corresponding to the laser heating during cutting, and comparison with measurements. Si and O elements were not considered in these calculations. Error bars (not visible) correspond to ± 10% of the values for the experimental data.

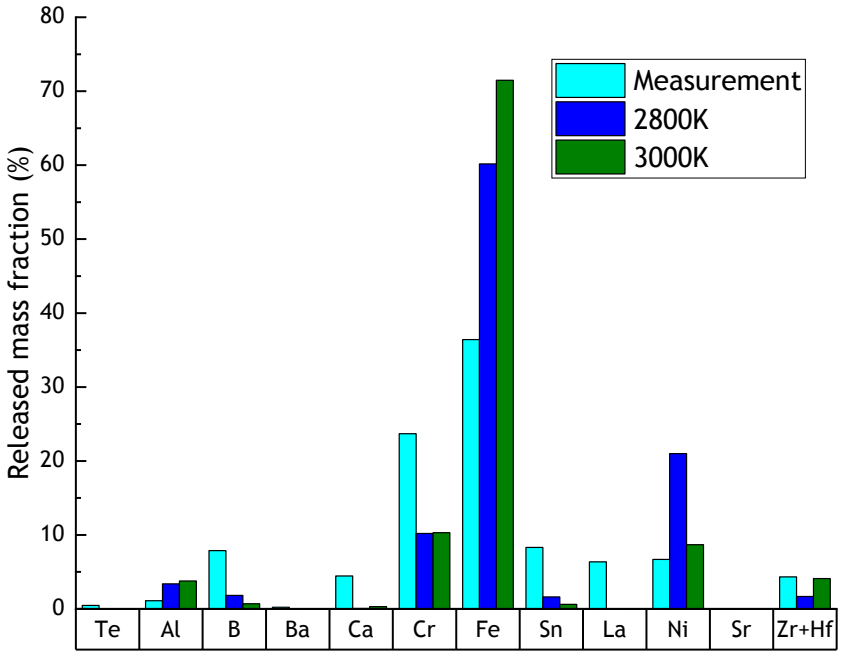

Figure 10 : Calculated mass fractions (minor elements) of aerosol released for an Ex-Vessel case study and for two temperatures corresponding to the laser heating during cutting, and comparison with measurements. Si and O elements were not considered in these calculations. Error bars (not visible) correspond to ± 10% of the values for the experimental data.

For the less volatile elements, Figure 10 compares computations and measurements. There is a clear underestimation of the released fraction of lanthanide, barium and strontium. This is only marginally modified by modifying the calculation temperature. Modification of the quantity of air in equilibrium with the heated fuel debris simulant was also not able to sufficiently increase the fraction of these elements while it affected the ratios of the major components. Even though these fission product elements contribute to only 11 wt% of the aerosols, they carry most of its radioactivity (see section 3.4).

Similarly, the aerosols released by laser cutting the In-vessel block correspond to the vapor proportions at 2900-3000K which is, in this case, only 200-300 K above liquidus. This hints that during laser cutting, the fuel debris material at the kerf is heated to a temperature of about 2900 K, which does not significantly depend on the block composition.

The effect of water has also been modelled. Considering a mass of water equal to 1.5 times the mass of the fuel debris melt, the best fit has been observed on the major releases. Nevertheless, even for a smaller mass of water (45% of the molten fuel), a large underestimation of nickel and silver (representing tellurium + palladium) releases (as for in-air case) has been noted.

These comparisons between experimental data and thermodynamic calculations in terms of chemical elements released during laser cutting indicate that the aerosol releases must mainly be controlled by a volatilization-condensation mechanism occurring at a temperature of 2800 to 3000 K. The effect of the gases (air/ water) in equilibrium with the cut material has also been observed. Nevertheless, there are some discrepancies for the minor elements. It is difficult to know whether these differences are due to shortcomings of the thermodynamic database or if they are due to deviations from thermodynamic equilibrium affecting some elements.

3.3 Mass and chemical element size distribution

One of the important information to obtain when characterizing aerosol in order to manage occupational exposures to inhalation of potential hazardous particles is to determine the number and/or mass size distribution. In top of that, associating the chemical composition to particle size is a clear added-value of such methodology, as explained previously in the Introduction section.

Figure 11 displays the chemical composition (in mass) according to the cut-off diameter associated to each stage of the DLPI® for Ex-Vessel and In-Vessel fuel debris simulants in air and underwater conditions. One can observe a clear predominance of the stainless steel elements (iron, chromium and nickel) and tin (from Zircalloy cladding) as previously seen in the paragraph above in the submicron sizes for any case. For air cutting conditions, Ex- Vessel is characterized by finer particles (around 100 nm) than the In-Vessel case (around 200 nm). IRSN reported in previous communication [20] that a mass median diameter (MMD) of 160 nm was found for Ex-Vessel and 270 nm for In-Vessel. A possible second mode can be mentioned for Ex-Vessel in air cutting conditions above 2 µm and concerns also stainless steel elements, in particular iron. For underwater conditions, the Ex-Vessel also

entails finer particle sizes than the In-Vessel with mass median diameter of 240 nm compared to 350 nm for In-Vessel. The increase in mass median diameter can be interpreted by more agglomeration of fine particles due to presence of water, this phenomenon being studied and explained through recent simulations [31]. Generally, these results are consistent with previous study of aerosols generated by laser cutting of stainless steel and characterized by submicron particle sizes [32].

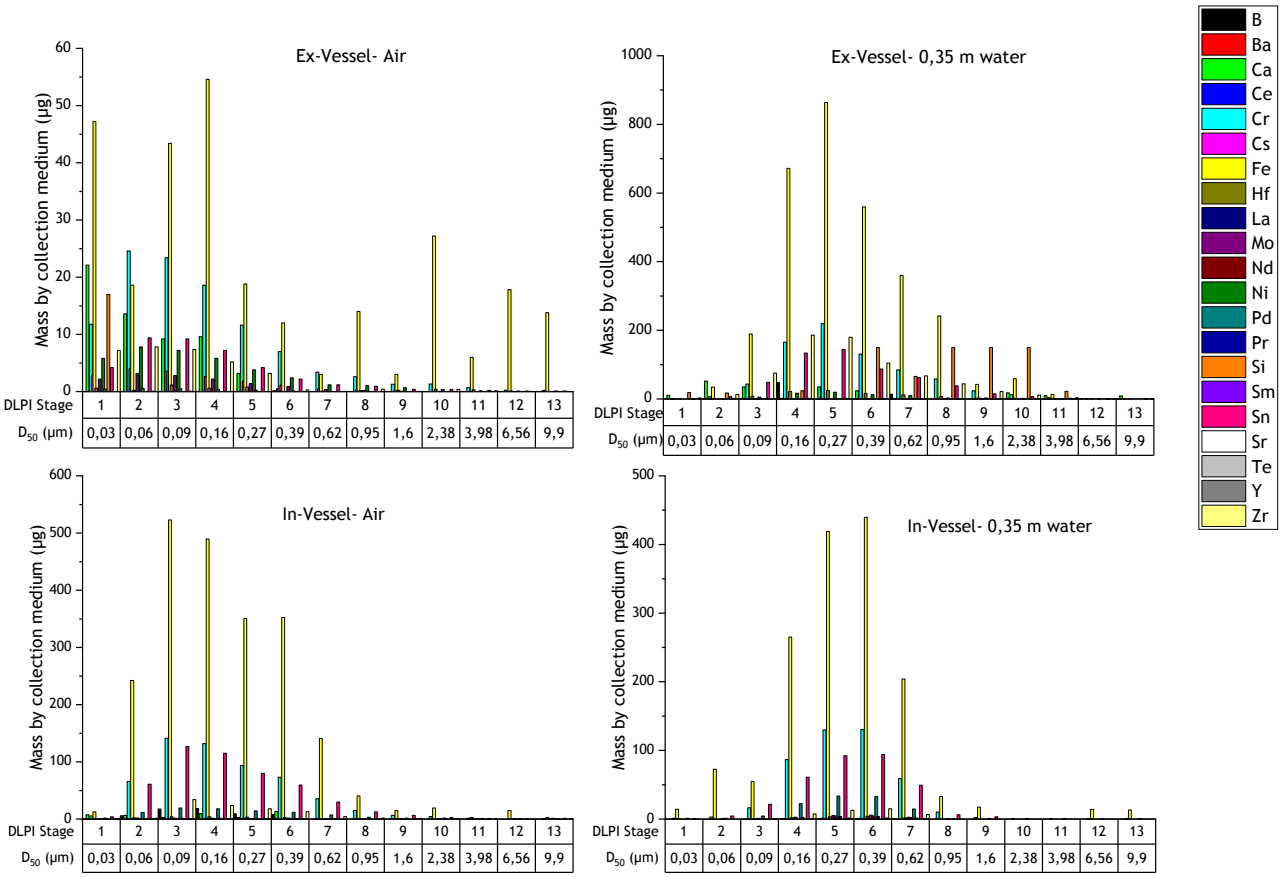

Figure 11 : Chemical mass size distributions of Ex-vessel and In-Vessel aerosols generated during laser cutting in air and underwater conditions. Error bars (not visible) correspond to ± 10% of the values.

3.4 Radioactivity and mass size distribution

One of the challenges stemming from this project is to be able to estimate the radioactivity that could be released from the measured elemental compositions for each laser cutting conditions and fuel debris simulants. Nishihara *et al* [33] calculated the isotope inventory and the associated radioactivity at different moments after the shutdown of the three damaged cores from Fukushima Daiichi. For the estimation, the sum of the masses and the sum of the activities of all isotopes of each element have been computed for F1 core (Ex-Vessel scenario). Their ratios are presented in Table S1 (Supplementary Material). Since the isotopic fractions are not much different between 1F1 and 1F2 (In-Vessel scenario) cores due to the presence of many other uncertainties, it have been decided to apply the same conversion ratios for both fuel debris simulant. The element concerned by the radioactivities are: Ba, Cs, La, Mo, Nd, Pd, Pr, Pu and transuranians (represented by Ce), Sm, Sn, Sr, Te, U (represented by Hf), Y, and Zr.

Figures 12 to 15 display the radioactivity distribution for the elements dosed on each DLPI® channel and which were not under the detection limits (from figures 12 to 15, radioactivity distribution for laser cutting of Ex-Vessel in air condition, Ex-vessel for underwater condition, In-Vessel in air condition and In-vessel for underwater conditions respectively). Figure 16 represents the cumulative radioactivity in percentage for the four laser cutting situations.

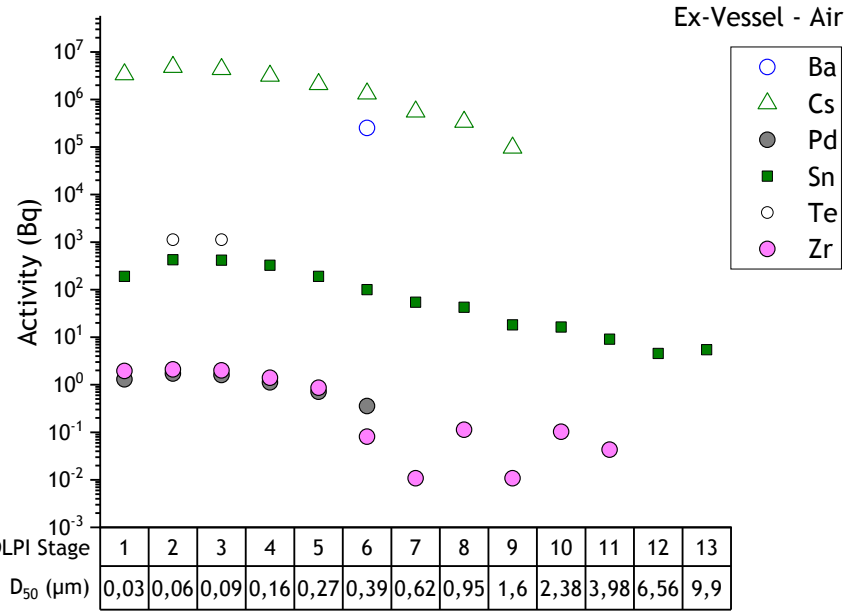

Figure 12 : Radioactivity distribution for significant elements dosed on the DLPI® collection substrate for laser cutting in air condition of Ex-Vessel. The equivalent radioactivity was calculated based on the masses obtained on each collection substrate and the conversion ratios (in Bq/g) indicated in the Table 1 ESI. DLPI® stages characterized by a lack of data means the mass on the collection substrate was under the detection limit and no conversion ratio was applied. Error bars (not visible) correspond to one standard deviation estimated to ± 10% based on the ICP-AES/MS dosing.

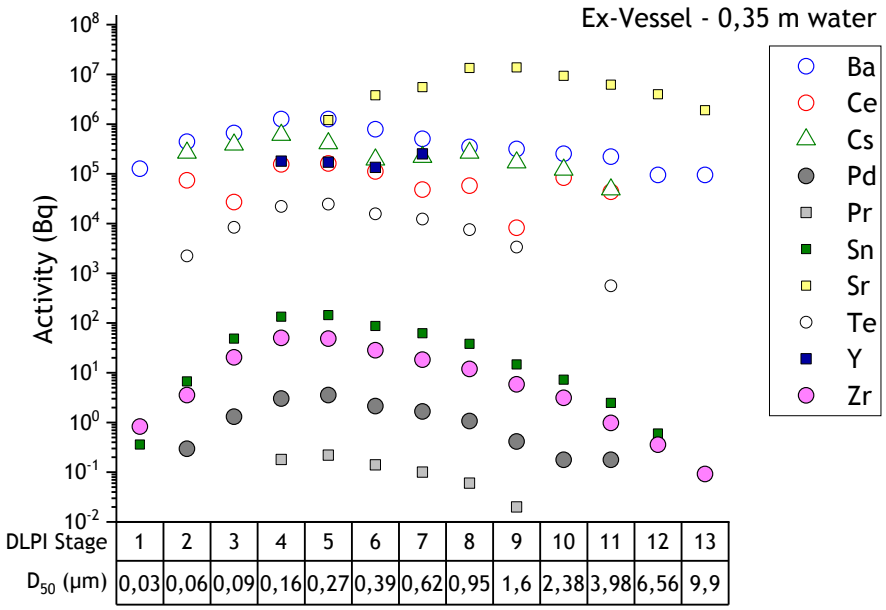

Figure 13 : Radioactivity distribution for significant elements dosed on the DLPI® collection substrate for laser cutting underwater condition of Ex-Vessel. The equivalent radioactivity was calculated based on the masses obtained on each collection substrate and the conversion ratios (in Bq/g) indicated in the Table 1 ESI. DLPI® stages characterized by a lack of data means the mass on the collection substrate was under the detection limit and no conversion ratio was applied. Error bars (not visible) correspond to one standard deviation estimated to ± 10% based on the ICP-AES/MS dosing.

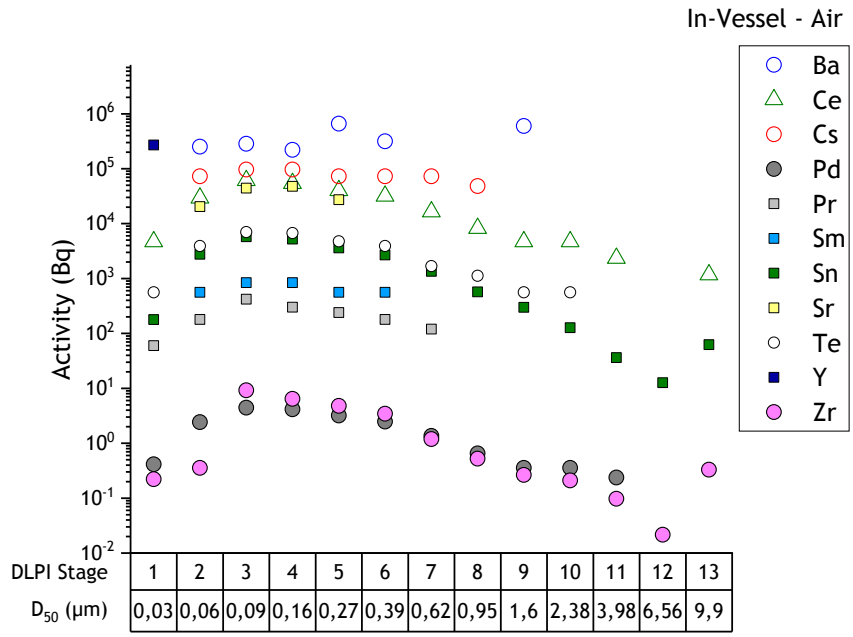

Figure 14 : Radioactivity distribution for significant elements dosed on the DLPI® collection substrate for laser cutting in air condition of In-Vessel. The equivalent radioactivity was calculated based on the masses obtained on each collection substrate and the conversion ratios (in Bq/g) indicated in the Table 1 ESI. DLPI® stages characterized by a lack of data means the mass on the collection substrate was under the detection limit and no conversion ratio was applied. Error bars (not visible) correspond to one standard deviation estimated to ± 10% based on the ICP-AES/MS dosing.

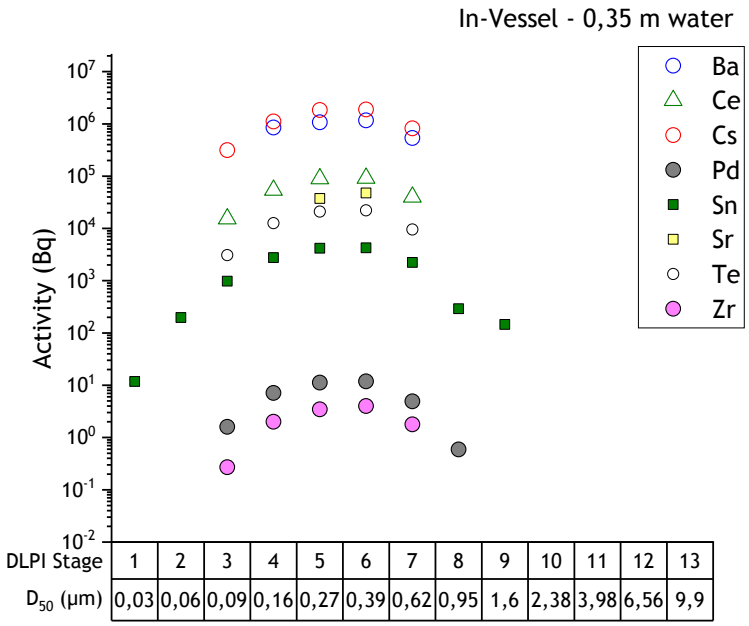

Figure 15 : Radioactivity distribution for significant elements dosed on the DLPI® collection substrate for laser cutting underwater condition of In-Vessel. The equivalent radioactivity was calculated based on the masses obtained on each collection substrate and the conversion ratios (in Bq/g) indicated in the Table 1 ESI. DLPI® stages characterized by a lack of data means the mass on the collection substrate was under the detection limit and no conversion ratio was applied. Error bars (not visible) correspond to one standard deviation estimated to ± 10% based on the ICP-AES/MS dosing.

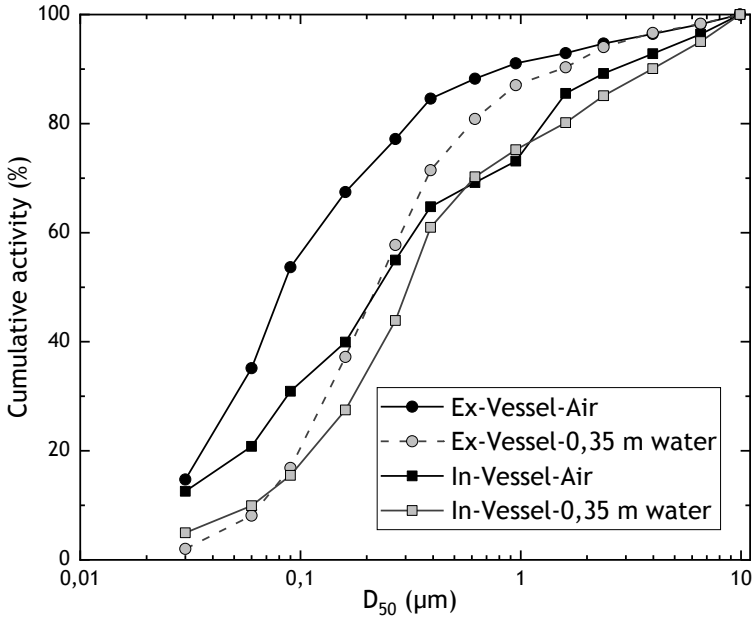

Figure 16 : Cumulative radioactivity for the four laser cutting conditions. Error bars (not visible) correspond to one standard deviation estimated to ± 10% based on the ICP-AES/MS dosing.

The size distributions representing radioelements (barium, caesium, palladium, tin, tellurium and zirconium) show for the in-air cutting of the Ex-vessel simulant (figure 12), a maximum around 60 nm for most the elements, except for barium (only detected at 0.39 µm). For underwater cutting of this Ex-vessel simulant (figure 13), the most abundant elements are barium, cerium (surrogate for plutonium), caesium and strontium. The maximum for several elements is achieved in the stage corresponding to a cutoff of 0.27 µm, also significantly higher that what was observed for the in air cutting. It must also be noted that there are significant masses of these elements (in particular cerium in the 2.38 µm stage) for the largest aerodynamic diameters. For the In-vessel simulant cut in air (figure 14), the most abundant elements (in terms of mass) are palladium (a lanthanide fission product) and cerium (surrogate for plutonium) detected on almost all DLPI® stages. The maximum of their presence is in the stage around 90 nm. Barium presents 2 local maxima (270-nm and 1.6 µm stages). Yttrium has only been detected in the stage corresponding to the smallest particles (<30 nm). For underwater In-vessel cutting (figure 15), all the elements display a peak close to 0.27 µm, which has been observed for the Ex-vessel case for underwater condition. Barium, cerium and caesium contribute to the most of the activity.

Regarding the cumulative activity (figure 16), for Ex-Vessel laser cutting in air conditions, 50% of the radioactivity is present in particles below 90 nm, and 99% below 950 nm. Caesium carries the largest part of the radioactivity at all sizes below 1 µm. At largest sizes, the role of zirconium and tin becomes dominant, but corresponds to a small fraction of the overall radioactivity. For Ex-Vessel underwater conditions, if we compare the DLPI® distribution to the cumulative radioactivity of the Ex-Vessel underwater laser cutting conditions, the distribution follows the same mass size distribution of cerium (simulating alpha particles, representing plutonium) with an aerosol median size around 300 nm. One can note that strontium carries most of the radioactivity for the particle sizes larger than 1 µm, while this element was not significant in the in-air cutting experiment.

For the In-Vessel laser cutting in air, the aerosol median size for the radioactivity is situated around 100 nm, with a maximum corresponding to the 90 nm DLPI® collection stage. 59% of the radioactivity is carried by strontium, 17% by barium and 16% by minor actinides (modelled by cerium) and 7% by the caesium. The contribution to radioactivity of sizes larger than or equal to 0.6 µm is significantly smaller than that in terms of mass. Nevertheless, it must be noted that for sizes above 1.6 µm, cerium representing alpha particles (surrogate of plutonium) is almost the only radioactivity-bearing element (96-97% of the radioactivity). Underwater conditions, the median size is situated around 300 nm but, beside this, the size distribution does not display major differences with in air laser cutting. The four laser cutting conditions evidence that small particles carry a significant radioactivity, mainly coming from cerium (representing plutonium), barium and caesium, even underwater cutting conditions.

These results combining characterization of chemical composition of potential radioactive aerosols and size distribution stress on the importance to implement this metrology. Ex-Vessel and In-Vessel do not show here important differences in terms of aerosol chemical composition and equivalent radioactivity. Both materials are characterized by fine airborne particles of stainless steel associated with radioactive isotopes carrying a non-negligible radioactivity. Even if the experimental campaign displays a significant variability in the chemical elements dosing which can be attributed to the heterogeneity of the studied fuel debris simulant, it leads to have a first approximate idea of type of aerosols that could be released in-situ in terms of chemical composition and size distribution for a

laser cutting technology implementation. Also other compositions of interest should be studied to cover a larger fraction of the expected fuel debris compositions to be dealt with during retrieval operations. Chae *et al* [10] reported in the case of stainless steel and ^{60}Co that the radioactivity distribution can follow the aerodynamic mass size distribution during laser cutting where submicron sized particles are generated. The cutting conditions can also affect the chemical composition and lead to modification of the size distribution. Nevertheless, it must be noted that in the current experiments in which a larger number of elements are considered, some radioisotopes are more present in the smallest aerosols (e.g. Ba, Cs) while others (Sr, Zr, Ce) are more present in the largest particles. The results presented here scope with suggestions proposed by Chae *et al* [10] such as implementing additional experimental study on the radioactive aerosol or considering of the actual radioactive elements related to the dismantling process. However, this study does not apply reproducibility assessment, but it would be very difficult due to the large heterogeneity of the fuel debris and of its simulants, contrary to the studies devoted to manufactured materials. Metrology robustness is necessary to use the data produced for developing and improving aerosol modelling in the laser cutting process.

3.4 Simulation of uranium

Hafnium has been considered as surrogate for uranium as the thermal properties of hafnium oxide (HfO_2 or hafnia) and uranium oxide (UO_2) are quite close. There are nevertheless limitations with the use of non-radioactive simulants of uranium dioxide [2]. They are mainly due to the very peculiar chemical characteristics of uranium, which has 4 oxidation states leading to the possible presence in the U-O system of the presence of many gaseous phases in the U-O system (U, UO, UO_2, UO_3 and O_2), so that the O/U ratio can evolve with temperature thanks to the release of gaseous UO or UO_3. Similar phenomena cannot be found with simulant materials.

Figure 17 presents two calculations using the procedure described in section 3.2 for the Ex-vessel sample. The unique difference is that each mole of uranium has been replaced by a mole of zirconium (representing hafnium). As hafnium is not present in the NUCLEA database, zirconium has been used

as a surrogate. Both elements are in the 4A column of Mendeleiev table. Their dioxides have full solubility for all phases (monoclinic, tetragonal-cubic and liquid) and their melting points are close (even if HfO_2 melts slightly at higher temperature: 2900°C vs 2690°C) [34].

We can see in figure 17 that uranium becomes the major element of the vapour phase and there is a 50-times increase in the computed mass fraction compared to the case with Hf (modelled by Zr). As uranium is the major element of vapour phase, it also affects the releases of other elements, not only by modifying the total vapour mass fraction: for instance, computed lanthanide and barium releases fractions are divided by 3, while boron releases are divided by 6. On the opposite, mass fractions of nickel and tellurium (modelled by silver) do not significantly vary between these two calculations.

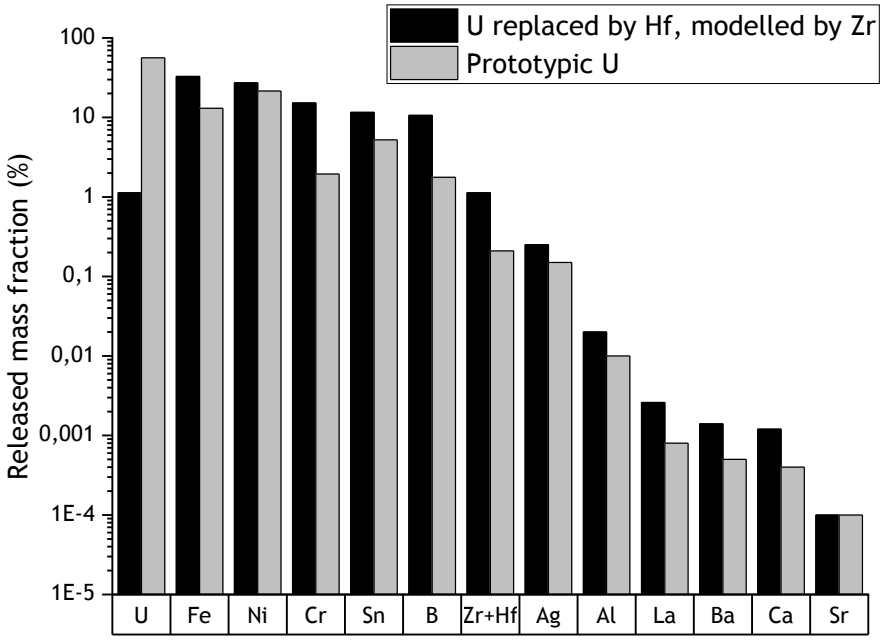

Figure 17 : Effect of uranium on the aerosol composition (Ex-vessel sample).

Similar calculations for the In-vessel sample composition give an increase in the uranium releases, but to a smaller extend (only by 3 times) compared to calculations with a simulant. It must be noted that the presence of uranium affects the release of other elements, as e.g. chromium, tin, lanthanum, barium and strontium releases increase while those of iron and boron decrease. This can be attributed to changes in the equilibrium repartition between the oxide and metal melts.

Uranium releases are computed for both configurations to have significant larger releases than those of hafnium. Indeed, hafnium had not been selected as a simulant for aerosol emission issues but to simulate the laser cutting capabilities. As there are still large uncertainties on these calculations, it would be relevant to conduct cutting tests on prototypic fuel debris simulants containing (depleted) uranium dioxide to confirm or infirm these results. An intermediate first test would be to collect and analyse aerosols above pools of molten fuel debris simulants with uranium or hafnium at 2800-3000 K.

Conclusion

In this work, we presented original aerosol characteristics combining chemical composition and particle size distributions obtained in the framework of Fukushima Daiichi dismantling projects in which laser cutting is developed by the French consortium ONET Technologies, CEA and IRSN laboratories. This work was implemented with two representative fuel debris simulants, and laser cutting were done in air and underwater conditions inside the DELIA facility hosted by the CEA. The fuel debris simulant aerosols were characterized through a dedicated sampling line including mass size distribution with cascade impactor (DLPI®) including post-sampling chemical analysis of the collection substrates, and mass concentration were determined with filter sampling and real time measurements (PPS-M®).

We showed that, for any condition given, fuel debris simulant aerosols are mainly composed of structural material elements, notably stainless steel elements (iron, chromium and nickel), corresponding to submicron particles. The aerodynamic mass median diameters obtained based on the cascade impactor measurements are comprised between 160 nm and 350 nm, with increasing of the aerodynamic mass median diameters when laser cutting are implemented underwater. When calculating the isotope inventory and the associated radioactivity for the fuel debris simulant, we evidenced that the submicron particles carry out a significant radioactivity, alpha particles (represented by cerium, surrogate of plutonium) follow the mass size distribution of radioelements, but other isotopes display important radioactivity such as strontium, caesium or barium. The data produced here

could already be used for modelling or designing development of strategies to implement in-situ the laser cutting for fuel debris retrieval and safety associated strategies, such mitigation means against aerosol dispersion using spray systems. Since these data have a significant impact on the safety measures to implement during dismantling, efforts should be done in this view for future experiments with representative radioactive material such as fuel debris simulant or eventually depleted samples.

Acknowledgements

This work has been carried out thanks to the subsidized project of Decommissioning and Contaminated Water Management (Development of Fundamental Technologies for Retrieval of Fuel Debris and Internal Structures) funded by the Japanese Ministry of Economy, Trade and Industry (METI) and managed by the Mitsubishi Research Institute (MRI). This project integrated research and development of the laser cutting technique for fuel debris retrieval for future in-situ application, characterization of aerosols released and dust collection technology. CEA-Cadarache was in charge of designing and synthesizing the two fuel debris simulants (representative of ex-vessel and in-vessel reactor configurations) on the PLINIUS platform, whereas CEA-Marcoule operated, for a part, the characterization of the bulk materials. The fuel debris simulants were then used on the DELIA facility located in the CEA-Saclay for implementation of the laser cutting. IRSN was in charge of the characterization of the aerosols released during laser cutting.

References

[1] Seibert. A, Staicu. D, Bottomley. D, Cologna. M, Boshoven. B, Hein. H, Kssim. E, Nourry. S, Ernstberger. M, Robba. D, Konoings. R. (2019) Thermophysical properties of U, Zr-oxides as prototypic corium materials, *Journal of Nuclear Materials*, 520, 165-177.

[2] Journeau. C, Roulet. D, Porcheron. E, Piluso. P, Chagnot. C. (2018) Fukushima Daiichi ful debris simulant materials for the development of cutting and collection technologies, *Journal of Nuclear Science and Technology*, 55 (9), 985-995.

[3] Mizokami, S. "Current Status and Recent Investigation Results of Fukushima Daiichi", presented at the 9th Conference on Severe Accident Research, Prague, Czech Republic, 2019.

[4] Pellegrini. M, Dolganov. K, Herranz. L.E, Bonneville. H, Luxat. D, Sonnenkalb. M, Ishikawa. J, Song. J.H, Gauntt. R.O, Fernandez Moguel. L, Payot. F, Nishi. Y. (2016) Benchmark Study of the Accident at the Fukushima Daiichi NPS: Best-Estimate Case Comparison, *Annals of Nuclear Technology*, 196:2, 198-210.

[5] Chagnot, C., Doyen, I., Li Puma, A., Georges, C., Porcheron, E., Gelain, T., Roulet, D., Deep gouging : Development of deep blind kerf laser cutting technology for Fukushima fuel debris retrieval, DEM,Avignon, France, 2018.

[6] George. C, Roulet. D, Chagnot. C, Journeau. C, Canneau. G, Blanchard. S, Porcheron. E. Benefits from developments in the field of Decommissioning for Controlled Laser Cutting Process, Proc WM2017 Conference, Phoenix, AZ, United States, 2017.

[7] ISO Standard 7708 (1995) Air Quality – Particle size fractions definitions for health-related sampling. Geneva: International Standards Organisation.

[8] Pilot. G, Fauvel. S, Gosse. X, de Dinechin. G, Vernhet. D. (2008) Measurement of secondary emissions during laser cutting of steel equipments, *Nuclear Engineering and Design*, 238, 2124-2134.

[9] Dodds. J.M and Rawcliffe. J. (2020) Radionuclide distribution during ytterbium doped fibre laser cutting for nuclear decommissioning, *Progress in Nuclear Energy*, 118, 103122.

[10] Chae. N, Lee. M-H, Choi. S, Park. B.G, Song. J-S. (2019) Aerodynamic diameter and radioactivity distributions of radioactive aerosols from activated metals cutting for nuclear power plant decommissioning, *Journal of Hazardous Materials*, 369, 727-745.

[11] Journeau. C, Monerris. J, Tormos. B, Brissonneau. L, Excoffier. E, Testud. V, Chagnot. C, Roulet. D, Fabricating Fukushima Daiichi in-vessel and ex-vessel fuel debris simulants for the development and qualification of laser cutting technique, European Review Mtg on Severe Accident Research, Warsaw, Poland, 2017.

[12] Nishihara. K, Iwamoto. H, Suyama. K. Estimation of fuel compositions in Fukushima Daiichi Nuclear Power Plant, JAEA Report JAEA Data/Code 2012-018.

[13] Samsonov G.V. The oxide handbook. IFI/PLENUM: New York: 1973.

[14] Capriotti, L., Quaini, A., Böhler, R., Boboridis, K., Luzzi, L., Manara, D. (2014) A laser heating study of CeO2 solid/liquid transition: challenges related to a refractory compound with a very high oxygen pressure. *High Temperature High Pressure*, 44, 69-82.

[15] Jégou, C., Boccaccio, E., Journeau, C., Piluso, P., & Monerris, J. Induction Heating simulation of Residual power in the VULCANO facility, *Proc. Int. Seminar Heating by Internal Sources,* Padova, Italy, 2001.

[16] Journeau. C, Piluso. P, Haquet. J.F, Boccaccio. E, Saldo. V, Bonnet. J.M, Malaval. S, Carénini. L, Brissonneau. L. (2009), Two dimensional interactions of corium with concretes: The VULCANO VB Test series, *Annals of Nuclear Energy*, 36 :1597-1613.

[17] Bouyer, V., Journeau, C., Haquet, J.F., Piluso, P., Nakayoshi, A., Ikeuchi, H., Washiya, T.,Kitagaki, T. "Large scale VULCANO Molten Core Concrete Interaction test considering Fukushima Daiichi conditions", 9th European Review Meeting on Severe Accident Research, Prague, Czech Republic, 2019.

[18] Ducros. G, Pontillon. Y, Malgouyres. P.P. (2013) Synthesis of the VERCORS experimental programme: Separate effect experiments on Fission Product Release, in support of the Phébus-FP program, *Annals of Nuclear Energy*, 61, 75-87, 2013.

[19] Chagnot. C, de Dinechin. G, Canneau. G. (2010) Cutting performance with new industrial continuous wave Nd : YAG highpower lasers : for dismantling of former nuclear workshops, the performances of recently introduced high power continuous wave Nd: YAG lasers are assessed, *Nuclear Engineering and Design*, 240, 2604-2613.

[20] Porcheron, E., Peillon, S., Gelain, T., Chagnot, C. Journeau, C., Roulet, D., Analysis of aerosol emission and dispersion during the laser cut-ting of Fukushima fuel debris simulants, ICONE 26, London, United Kingdom, 2018.

[21] Baron. P.A and Willeke. K. (2001) Aerosol measurement-Principles. Techniques and applications (2nd Edition). Wiley Interscience.

[22] Brock T.D. (1983) Membrane Filtration: A User's Guide Reference Manual, Science Tech, Inc., Madison, WI.

[23] Soo. J.-C, Monaghan. K, Lee. T, Kashon. M, Harper. M. (2015) Air sampling filtration media: Collection efficiency for respirable size-selective sampling, *Aerosol Science and Technology*, 50 (1). 76-87.

[24] Zikova. N, Ondráček. J, Ždímall. V. (2015) Size-Resolved Penetration Through High-Efficiency Filter Media Typically Used for Aerosol Sampling. *Aerosol Science and Technology*. 49. 239-249.

[25] Chiari. M, Yubero. E, Calzolai. G, Lucarelli. F, Crespo. J. (2018) Comparison of PIXE and XRF analysis of airborne particulate matter samples collected on Teflon and quartz fiber filters. *Nuclear*

[26] Amanatidis. S, Matti Maricq. M, Ntziachristos. L. (2016) Measuring number, mass, and size of exhaust particles with diffusion chargers: The dual Pegasor Particle Sensor, *Journal of Aerosol Science*, 92, 1-15.

[27] Rostedt. A, Arffman. A, Janka. K, Ojanper. J-Y, Keskinen. J. (2014) Characterization and Response Model of the PPS-M Aerosol Sensor, *Aerosol Science and Technology*, 48, 1022-1030.

[28] Bakardjieva. S, Barrachin. M, Bechta. S, Bottomley. D, Brissonneau. L, Cheynet. B, Fischer.E, Journeau. C, Kiselova. M, Mezentseva. L, Piluso. P, Wiss. T. (2010) Improvement of the European thermodynamic database NUCLEA, *Progress in Nuclear Energy*, 52, 84–96.

[29] Journeau, C., Zanini, J., Excoffier, E., Testud, V., Brackx, E., Chagnot, C., Doyen, I. Porcheron, E., Roulet, D. "Aerosols released during the laser cutting of a Fukushima Daiichi debris simulant", 9th European Review Meeting on Severe Accident Research, Prague, Czech Republic, 2019.

[30] Piluso. P, Monerris. J, Journeau. C, Cognet. G. (2002) Thermophysical properties of liquid UO2, ZrO2 and corium by molecular dynamics and predictive models, *International Journal of Thermophysics*, 23, 1229–1240.

[31] Gelain, T., Chagnot, C., Porcheron, E., Roulet, D. "CFD simulations of aerosol dispersion and agglomeration during the laser cutting of Fukushima fuel debris simulants," in Proceedings of the 2018 26th International Conference on Nuclear Engineering ICONE26, London, United Kingdom, 2018.

[32] Peillon. S, Fauvel. S, Chagnot. C, Gensdarmes. F. (2017) Aerosol Characterization and Particle Scrubbing Efficiency of Underwater Operations during Laser Cutting of Steel Components for Dismantling of Nuclear Facilities, *Aerosol and Air Quality Research*, 17, 1363-1373.

[33] Nishihara. K, Iwamoto. H, Suyama. K. Estimation of fuel compositions in Fukushima Daiichi Nuclear Power Plant, JAEA Report JAEA Data/Code 2012-018.

[34] Ruh, R., Garett, H.J., Domaglia, R.F., Tallan, N.M. (1968) The system zirconia-hafnia, *Journal of American Ceramic Society*, 51, 23-27.